Machine Learning Discrimination and Ultrasensitive Detection of Fentanyl Using Gold Nanoparticle-Decorated Carbon Nanotube-Based Field-Effect Transistor Sensors

Wenting Shao,[1] Dan C. Sorescu,[2,3] Zhengru Liu,[1] and Alexander Star*[1,4]

1. Department of Chemistry, University of Pittsburgh, Pittsburgh, Pennsylvania 15260, United States

2. United States Department of Energy, National Energy Technology Laboratory, Pittsburgh, Pennsylvania 15236, USA

3. Department of Chemical & Petroleum Engineering, University of Pittsburgh, Pittsburgh, Pennsylvania 15261, USA

4. Department of Bioengineering, University of Pittsburgh, Pittsburgh, Pennsylvania 15261, United States

** Correspondence author email: astar@pitt.edu*

Abstract

The opioid overdose crisis is a global health challenge. Fentanyl, an exceedingly potent synthetic opioid, has emerged as a leading contributor to the surge in opioid-related overdose deaths. The surge in overdose fatalities, particularly due to illicitly manufactured fentanyl and its contamination of street drugs, emphasizes the urgency for drug-testing technologies that can quickly and accurately identify fentanyl from other drugs and quantify trace amount of fentanyl. In this paper, gold nanoparticle (AuNP)-decorated single-walled carbon nanotube (SWCNT)-based field-effect transistors (FETs) were utilized for machine learning-assisted identification of fentanyl from codeine, hydrocodone, and morphine. The unique sensing performance of fentanyl led us to use machine learning approaches for accurate identification of fentanyl. Employing linear discriminant analysis (LDA) with a leave-one-out cross-validation approach, we achieved a validation accuracy of 91.2%. Meanwhile, density functional theory (DFT) calculations revealed the factors that contributed to the enhanced sensitivity of the Au-SWCNT FET sensor toward fentanyl as well as the underlying sensing mechanism. Finally, fentanyl antibodies were introduced to the Au-SWCNT FET sensor as specific receptors, expanding the linear range of the sensor in the lower concentration range, and enabling ultrasensitive detection of fentanyl with a limit of detection at 10.8 fg mL^{-1}.

1. Introduction

The misuse of synthetic opioids for non-medical purposes is currently driving public health crises in many countries. These substances pose a substantial challenge due to their ready availability and cheap production. Especially, illicit fentanyl is driving the recent surge in drug overdose deaths in the United States. At the same time, there has been a growing trend of using fentanyl as an adulterant in other illicit drugs to increase the potency of the drug, further elevating the likelihood of fentanyl-related overdose deaths.[1] Therefore, it is crucial for the development of fentanyl-testing technologies to find systems that can quickly and accurately identify fentanyl from other drugs and quantify trace amount of fentanyl.

For a long time, gas chromatography mass spectrometry (GC-MS) and liquid chromatography-tandem mass spectrometry (LC-MS/MS) have been the standard practice for quantitative detection of fentanyl in many laboratories.[2] Spectroscopic methods, such as infrared (IR) spectroscopy and Raman spectroscopy, are also thought to provide high selectivity through structural information.[3] In particular, surface-enhanced Raman scattering (SERS), which greatly amplifies the Raman scattering signal of sample molecules by using a plasmonic substrate, has emerged as a powerful technique for the sensitive detection of fentanyl as it offers rapid, label-free and even portable detection.[4] Nevertheless, certain limitations persist with this technique, including limited quantification capabilities which are less suitable for high-throughput screening.

Electrochemical methods are generally considered to be rapid, easy-to-use, and low-cost alternatives, making them particularly attractive for on-site quantitative analysis. So far, electrochemical detection of fentanyl has shown promising results as an alternative to chromatographic and spectroscopic methods.[5] In this work, we aim to further enhance the specificity of fentanyl detection using an electrochemical sensor and achieve ultrasensitivity down to femtomolar level. To achieve this goal, carbon nanotube (CNT)-based field-effect transistors (FETs) were chosen for the development of fentanyl sensors. CNT-based FETs not only show high sensitivity and low limit of detection toward a wide spectrum of analyte, but also provide valuable insights into the mechanisms governing the sensor responses.[6] The rich information garnered through the FET sensors has enabled us to identify multiple characteristics of sensor responses, ultimately enabling the utilization of machine learning methodologies for the discrimination and differentiation of distinct analytes.[7]

Herein, AuNP-decorated SWCNT-based FET sensors were employed for machine leaning-assisted identification of fentanyl from codeine, hydrocodone, and morphine (Figure 1a). Distinctive sensing performance was observed for fentanyl, which led us to use machine learning approaches for accurate identification of fentanyl. A total of 15 features were extracted from the FET transfer characteristics for model training, and by applying a linear discriminant analysis (LDA) with leave-one-out cross-validation, a validation accuracy of 91.2% was achieved. Next, to uncover the factors that contribute to the selectivity and enhanced sensitivity of the Au-SWCNT FET sensors toward fentanyl, a theoretical study based on density functional theory (DFT) calculations was carried out to explore the molecular-level interactions between this opioid and the Au-SWCNT hybrid structure. Finally, ultrasensitive detection with a limit of detection of 10.8 fg mL^{-1} was achieved by immobilizing fentanyl antibodies on AuNPs. The addition of specific antibodies also leads to high specificity of the FET sensor.

2. Results and Discussion

Figure 1b shows a schematic illustration of an Au-SWCNT FET device. Specifically, high purity semiconductor-enriched (sc-) single-walled carbon nanotubes (SWCNTs) were employed as the semiconducting channels of the FET sensor as they offer high on-off ratio for FETs as well as a platform for chemical functionalization. Sc-SWCNTs were deposited between the interdigitated source and drain electrodes (channel length: 10 μm) on a Si/SiO_2 substrate via dielectrophoresis. The surface morphology of the FET device was characterized by atomic force microscopy (AFM), from which a densely interconnected network of sc-SWCNTs could be observed, with an average diameter of the sc-SWCNTs of 1.7 ± 0.5 nm (Figure 1c). AuNPs were decorated on the sc-SWCNTs via bulk electrolysis, where they nucleated preferentially on the oxygen-containing defect sites of the SWCNTs due to the higher surface energy.[8] The resulted AuNPs have an average height of 43.1 ± 1.2 nm (Figure 1d). The nucleation of AuNPs on sc-SWCNTs also alters the FET transfer characteristics, which was evidenced by the increase in the source-drain current (I_d) of the FET device (Figure S1).

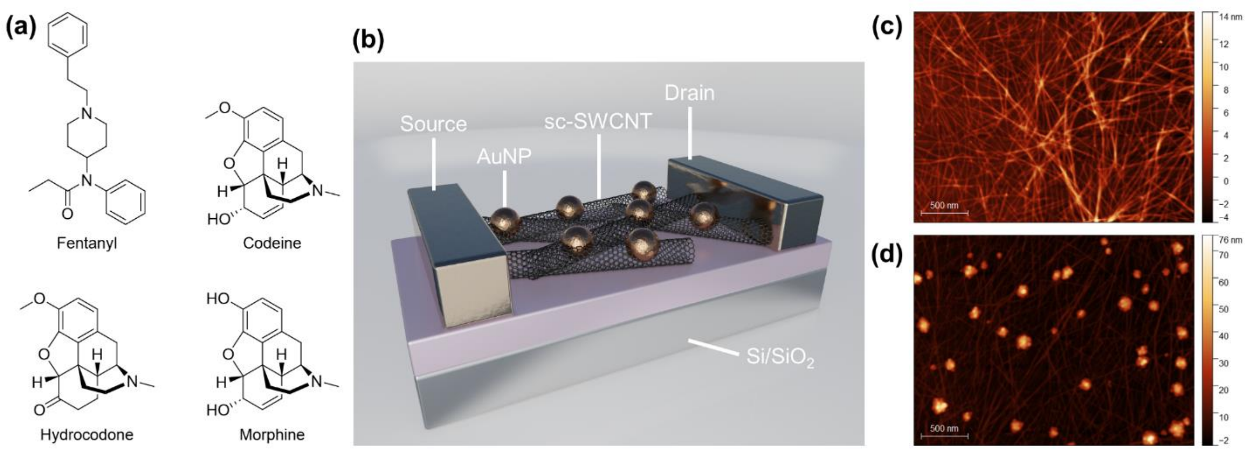

Figure 1. Detection of opioid drugs using a AuNP-decorated sc-SWCNT-based FET device. (a) Molecular structures of fentanyl, codeine, hydrocodone, and morphine. (b) Schematic illustration of a AuNP-decorated sc-SWCNT-based FET device. (c) AFM image of bare sc-SWCNTs deposited between the source and drain electrodes. (d) AFM image of AuNP-decorated sc-SWCNTs.

The binding of fentanyl on Au surfaces relies on the interactions between the lone pairs of N and O atoms and Au atoms, as well as the π-metal interactions between aromatic rings of fentanyl and AuNP surfaces.[4b, 9] AuNP-decorated SWCNTs prove to be an exceptional substrate for SERS, facilitating the detection of molecules binding to the Au surfaces.[10] However, although we observed a substantial increase in the Raman signal of SWCNTs following the decoration with

AuNPs, demonstrating SERS capability inherent in Au-SWCNT devices, no characteristic peaks corresponding to fentanyl were discerned after the incubation with the substance (Figure S2). In contrast, the binding of fentanyl on AuNPs can be effectively captured by SWCNT-based FET sensors employing a liquid-gated FET configuration. In Figure 2a, changes in the transfer characteristics of the Au-SWCNT FET device, induced by incubation with increasing concentrations of fentanyl, are illustrated. A consistent drop in the source-drain current was observed, indicating the decrease in the conductance of the semiconducting channels. To further validate the fentanyl sensing capabilities, a calibration plot was constructed using the absolute relative I_d changes at $V_g = –0.3$ V. Analysis of the calibration curve shows that the linear range of the fentanyl FET sensor spans from 2 µg mL^{-1} to 50 µg mL^{-1}, and the calibration sensitivity of the sensor is 0.135 (Figure 2b). Moreover, a dissociation constant (K_d) of 2.0 µM can also be extracted from the sensor responses (Figure S3).[11]

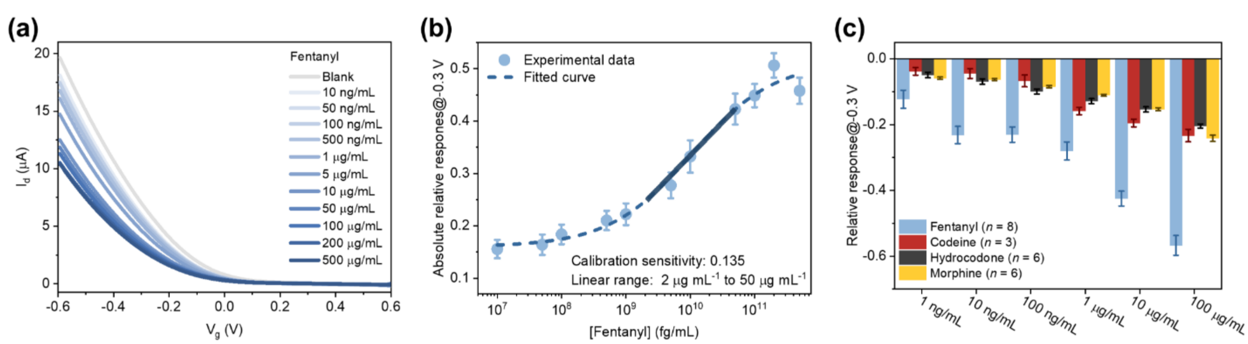

Figure 2. Fentanyl sensing performance of the Au-SWCNT FET device. (a) FET transfer characteristics of the Au-SWCNT FET device upon adding increasing concentrations of fentanyl from 10 ng mL^{-1} to 500 µg mL^{-1}. (b) Calibration plot for fentanyl detection. The concentration of fentanyl indicated on x-axis is plotted on a logarithmic scale. The linear range is indicated using a solid line. (c) Comparison of sensor responses for fentanyl, codeine, hydrocodone, and morphine. All error bars were calculated from multiple devices. The number of devices (n) used for calculation is indicated in parentheses in the legend.

Using the same Au-SWCNT FET methodology, sensor responses were recorded for several other opioids, namely codeine, hydrocodone, and morphine. Like fentanyl, these three opioid drugs contain N and O atoms as well as aromatic rings, enabling them to interact with AuNPs and consequently alter the transfer characteristics of SWCNTs in a similar way. However, the comparison of the sensor responses clearly demonstrates that the Au-SWCNT FET devices not only yielded the largest response for fentanyl at the same concentration level, but also exhibited higher sensitivity and superior sensing capabilities for the detection of fentanyl (Figure 2c). Although we observed distinct sensing behavior in Au-SWCNT FET sensors during fentanyl detection (Figure S4), it is important to note that the interactions between opioid drugs and AuNPs are non-specific. The lack of specificity led us to employ a supervised machine learning algorithm to discriminate between fentanyl and other opioid drugs. Our dataset encompassed sensing data from 56 FET devices for fentanyl and 126 FET devices for other opioids, and for each FET device we extracted 15 features from the sensing dataset, *i.e.*, FET transfer characteristics before and after incubation with the opioid drug (Figure S5).[8c] These features reflect the changes of the electrical properties of the FET devices and are associated with various possible sensing mechanisms.[12] A linear discriminant analysis (LDA) model was used for model training, and the classification model accuracy was verified by leave-one-out cross-validation. Notably, the validation accuracy reached an impressive 91.2%, demonstrating the ability of Au-SWCNT FET devices to effectively discriminate fentanyl from the other opioids (Table 1).

Table 1. Validation accuracy for the classification of fentanyl and other opioids using LDA.

Class	Predicted as fentanyl	Predicted as other opioids	Accuracy
Fentanyl	45	11	0.912
Other opioids	5	121	

The different sensing behaviors observed for fentanyl relative to the other opioids tested here suggest distinctive interaction patterns between these opioid drugs and AuNPs. To shed light on the unique fentanyl sensing capabilities exhibited by Au-SWCNT FET devices, we conducted theoretical studies based on dispersion-corrected first principles density functional theory (DFT) calculations[13] to investigate the adsorption of opioid drugs on Au surfaces.

The complexity of the real Au nanoparticles used in experiments is hard to be entirely captured in simplified computational models that can be evaluated based on DFT computational methods. Nevertheless, we considered several models that include the main characteristics for large size Au nanoparticles as well as hybrid models characteristic to Au nanoparticles (AuNP) deposited on SWCNT. For this purpose, three specific models have been analyzed, namely, an extended bare Au(111) surface and a Au(111) surface with an extra Au adatom (ad) which are representative for large size Au nanoparticles as well as a model containing a heterogeneous system composed of a Au(80) nanoparticle adsorbed on a (14,0) SWCNT at an O-functionalized defect. For all three models, the adsorption properties of fentanyl, codeine, hydrocodone and morphine molecules have been determined by analyzing different binding orientations and adsorption at different surfaces sites. A summary of the most stable configurations identified are illustrated in Figures S5 and S6 for the case of adsorption on bare Au(111) surface, respectively, when adsorption is mediated by a Au(ad)/Au(111). The corresponding adsorption energies for each of the molecular systems analyzed are summarized in Figure 3a. On the bare Au(111) surface the most stable binding orientations correspond to configurations that maximize the attractive dispersion interactions between individual atoms of the molecules and surface atoms. Such interactions are maximized in the case of fentanyl where the molecule adsorbs in a lying down configuration which allows the majority of O, N or C atoms of the aromatic rings to become spread on the surface, in close proximity to Au atoms. This characteristic is distinct from the case of the other three adsorbed molecules where a larger proportion of atoms are located at larger separation from the surface, pointing away from it, where their interaction with Au surface atoms is reduced. As a result, an increase in attractive van der Waals interaction with surface atoms is present for fentanyl which is characterized by an adsorption energy of 62.5 kcal mol^{-1}, value higher by at least 20.1 kcal mol^{-1} than those of the other three molecules analyzed (Figure S6). On the other hand, in consistence with the experimental findings where comparable sensor responses were observed for the codeine, hydrocodone and morphine group (hereafter denoted as group II of molecules), the corresponding adsorption energies are very close to each other and are distributed in a relatively narrow range of values, *i.e.,* 38.1–42.2 kcal mol^{-1}, making their energetic differentiation more difficult.

Au adatoms which can be extracted either from the bulk or from the surface edges or steps, can be also present on Au(111) surface and they can influence significantly the adsorption properties of organic molecules co-adsorbed on the surface. Our structural and energetic results from Figures 3a and S6 confirm this aspect. In particular, an increase in binding energies is seen for all molecular systems in the case of adsorption mediated by Au adatom relative to the case of the bare surface. The presence of Au adatoms allows formation of new covalent bonds, primarily with N atoms of the molecules as seen in panels a–c of Figure S7, or present an enhanced interaction with C atoms of the aromatic rings as is the case for morphine, as shown in panel d of Figure S7. The energetic data in Figure 3a demonstrates, however, that despite the increase in adsorption energies, the stability order is not modified relative to the case of bare Au surface, with fentanyl being more stable by at least 20.2 kcal mol^{-1} relative to group II of molecules. Additionally, the presence of Au adatoms does not lead to significant differentiation in binding energies of the group II of molecules which remain closely separated in the 49.9–51.1 kcal mol^{-1} range. Furthermore, we note that the increased stability of fentanyl relative to the other three molecules from group II is valid not only for the most stable configuration depicted in panel a of Figure S7 but also for other less favorable Au(ad)-fentanyl configurations. This aspect is illustrated in Figure S8 where it is shown that independent on the specific location of Au(ad) around fentanyl molecule where interactions with different groups of fentanyl atoms takes place, all the resulted configurations have adsorption energies substantially larger than those of group II of molecules.

Extension of computational analysis to the case when molecular adsorption takes place on a hybrid AuNP-SWCNT system leads to similar findings. The most stable configurations identified in this case and depicted in Figure 3b, show molecular conformations that maximize dispersion interactions with Au atoms of the nanoparticle. Additionally, formation of new bonds between the apex Au atoms of the metallic nanoparticle and the lone pair containing N atoms of the molecules can be observed. For these configurations a general shift in adsorption energies relative to the values observed on either bare or Au-adatom mediated surfaces takes place, effect due to a decrease in the long range attractive vdW dispersion interactions relative to the extended, infinite slab models analyzed above. This energetic shift, however, does not change the relative stability order of molecules with fentanyl remaining the most stable system by 15.7-16.7 kcal mol^{-1} relative to group II of molecules. Taking in totality, the computational results obtained demonstrate that independent on the specific surface model considered, *i.e.* the bare Au(111) or Au(ad)/Au(111) slabs, or the hybrid AuNP/SWCNT model, fentanyl is characterized by the highest binding energy, well-separated by at least 15–20 kcal mol^{-1}, depending on the specific surface characteristics, from the binding energies of group II of molecules investigated. For the codeine, hydrocodone and morphine molecules with their bulky molecular conformations which makes difficult simultaneous interaction of majority of their N, O and aromatic ring C atoms with Au surface, there is little difference in their relative stabilities, with a slight preference for codeine relative to hydrocodone and morphine, particularly seen for the extended bare Au(111) surface.

To gain further understanding of the sensing mechanism upon fentanyl binding to AuNP-SWCNT, we detail the charge transfer taking place at the interfaces of the fentanyl-AuNP/SWCNT system. For the interface between fentanyl and AuNP (Figure 3c), it can be seen that charge redistribution takes place both in the region of the Au-N bond as well as between C atoms of the aromatic ring and Au surface. In this case, a total Bader charge of 0.35 e was determined to be transferred from the molecule to the AuNP/SWCNT system. For the interface between fentanyl-AuNP and SWCNT (Figure 3d), the charge redistribution is particularly localized in the region of the functionalized defect on the SWCNT surface where Au nanoparticle is anchored on the SWCNT. A total Bader charge of 0.42 e was found to be transferred from fentanyl-AuNP system to the SWCNT. Due to the p-type semiconductor characteristic of the SWCNT, this charge transfer from fentanyl-AuNP system into the SWCNT induced an n-doping effect, thereby contributing to the observed decrease in the device conductance during the sensing experiment (Figure 2a).

Additional details of the electronic properties of fentanyl adsorbed on AuNP/SWCNT are indicated in Figure 3f where the total density of states of the entire system is represented together with individual localized density of states of fentanyl (F), AuNP and SWCNT subsystems. As shown in this figure, there are nonzero contributions of the electronic levels just above the Fermi level. These contributions emerge from the delocalized charge density involving multiple groups of atoms on both AuNP and SWCNT as shown in Figure 3e.

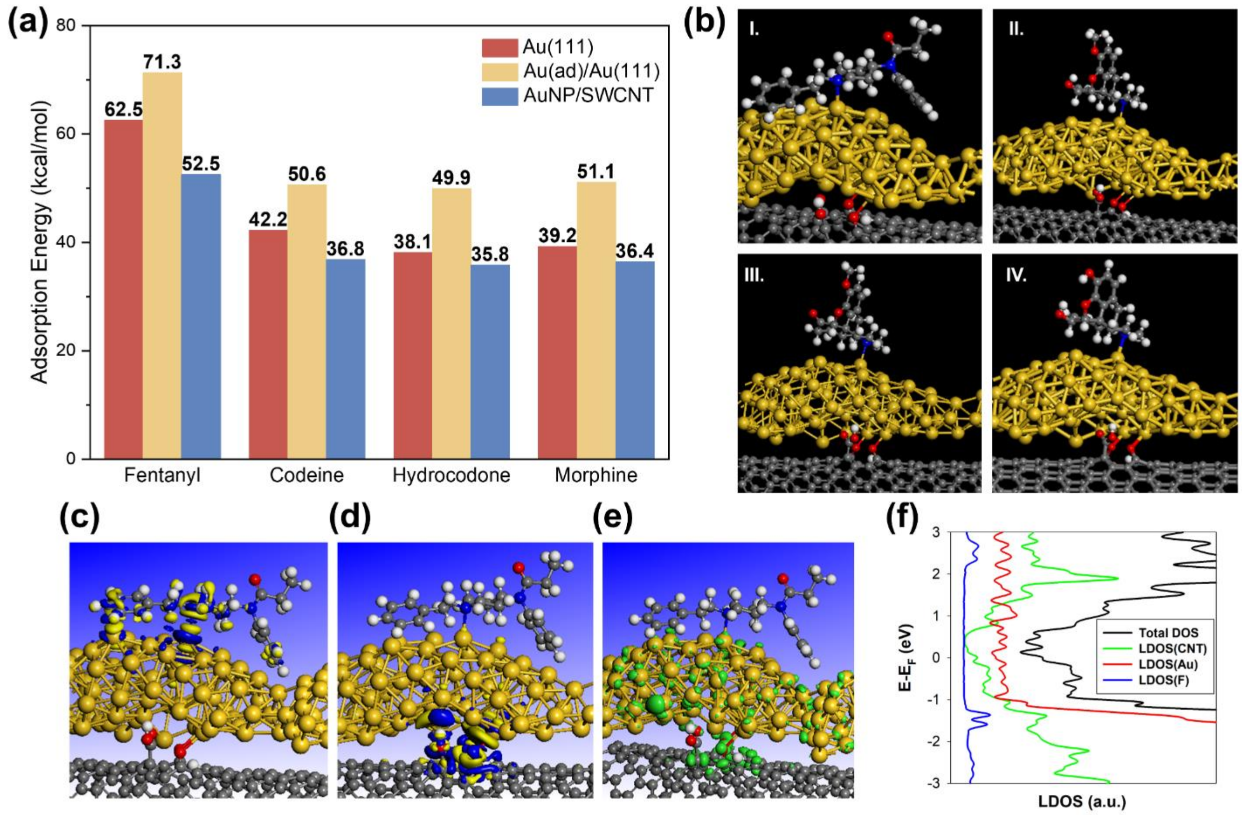

Figure 3. Results of DFT calculations for the adsorption of opioid molecules on Au-SWCNTs. (a) Comparison of the calculated adsorption energies (kcal mol^{-1}) on Au(111), Au(ad)/Au(111) and AuNP/SWCNT systems. (b) Results of DFT calculations illustrating the most stable adsorption configurations on AuNP/SWCNT for: I. fentanyl; II. codeine; III. hydrocodone; IV. morphine Charge difference maps for fentanyl adsorbed on Au/SWCNT at (c) the interface between the fentanyl and AuNP-SWCNT system, respectively, at (d) the interface of fentanyl-AuNP system with SWCNT. The indicated yellow and blue isosurfaces correspond to values of $\pm$ 0.01 e$^-$ Å^{-3}. (e) The partial charge density isosurface (0.01 e$^-$ Å^{-3}) of the electronic levels located within 0.2 eV above the Fermi level. (f) Total density of states for fentanyl adsorbed on AuNP/SWCNT and the local density of states (LDOS) projections for SWCNT, AuNP, and fentanyl (F) molecule.

When the fentanyl concentration fell below 10 ng mL^{-1}, interactions between fentanyl and AuNPs, as well as bare sc-SWCNTs, failed to produce substantial sensor responses. Consequently, the FET devices exhibited minimal sensitivity to fentanyl in this concentration range (Figure S9). To expand the linear range of the Au-SWCNT FET sensor and enable ultrasensitive fentanyl detection capabilities, fentanyl antibodies were introduced for the specific identification of fentanyl.

In this sensor configuration, fentanyl antibodies were anchored onto the surface of AuNPs, allowing the Au-SWCNT FET devices to probe the specific binding interactions between fentanyl and the fentanyl antibody. Illustrated in Figure 4a, the binding of fentanyl to the antibody led to a reduction in the conductance of the FET device. As previously reported, this binding process relies on nonpolar hydrogen–π interactions and cationic-π interactions between fentanyl and amino acid residues within the binding sites of the antibody such aspartate (Asp) and tyrosine (Try).[14] This interaction results in an alteration in the charge distribution of the antibody, leading to a decrease in the work function of the AuNPs[15] and a corresponding increase in the Schottky barrier at the junction of the AuNPs and SWCNTs,[16] hence the decrease in the conductance of the FET devices (Figure 4b). This observation also aligns with results of our prior study employing norfentanyl antibody-functionalized Au-SWCNT FET sensors for norfentanyl detection, where a similar antibody binding process occurred during the sensing experiment.[17]

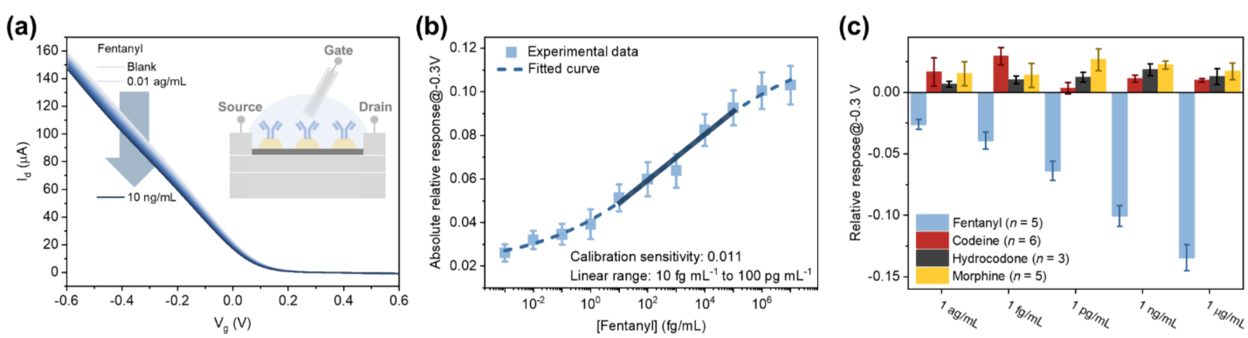

Figure 4. Fentanyl sensing performance of the fentanyl antibody-functionalized Au-SWCNT (fentanyl-ab@Au-SWCNT) FET device. (a) FET transfer characteristics of the fentanyl-ab@Au-SWCNT FET device upon adding increasing concentrations of fentanyl from 1 ag mL^{-1} to 10 ng mL^{-1}. Inset shows the sensor configuration. (b) Calibration plot for fentanyl detection. The concentration of fentanyl indicated on x-axis is plotted on a logarithmic scale. The linear range is denoted using a solid line. (c) Comparison of sensor responses for fentanyl, codeine, hydrocodone, and morphine. All error bars were calculated from multiple devices. The number of devices (*n*) used for calculation is indicated in the parentheses in the legend.

The introduction of fentanyl antibody to the sensor design resulted in an expanded linear range in the lower concentration range. From the calibration curve, a calibration sensitivity of 0.011 and a linear range from 10 fg mL^{-1} to 100 pg mL^{-1} can be determined. Furthermore, the fentanyl antibody-functionalized Au-SWCNT FET sensor exhibited a limit of detection (LOD) of 10.8 fg mL^{-1} (32.1 fM), demonstrating ultrasensitivity of the FET sensor and outperforming other electrochemical fentanyl sensors reported in the last 5 years (Table S1). The ultrasensitivity can be attributed to the strong binding affinity between fentanyl and fentanyl antibody.[14, 18] In our study, this strong binding, occurring at the sensor surface, can also be supported by the low dissociation constant of 1.2 pg mL^{-1} (3.6×10^{-12} M), as extracted from the calibration curve depicted in Figure 4b. The stronger binding between fentanyl and its antibody, compared to the binding between fentanyl and bare AuNPs, facilitated probing of fentanyl interactions on the sensor surface at significantly lower concentrations.

Additionally, the incorporation of fentanyl antibodies as the specific recognition element on the sensor surface introduces good specificity to the FET sensor. When comparing sensor responses for fentanyl, codeine, hydrocodone, and morphine, the fentanyl antibody-functionalized FET sensor exclusively exhibits sensitivity to fentanyl (Figure 4c). The small positive sensor responses observed with the opioid drug molecules from group II likely stemmed from the non-specific interactions between these molecules and bare SWCNTs, as evidenced by similar positive responses observed in Figure S9 when fentanyl was added to FET devices with bare SWCNTs. Even when testing fentanyl in the presence of the other three opioid drugs, the fentanyl-ab@Au-SWCNT FET devices retained their sensing capability for fentanyl, showing high specificity and good resistance to interfering opioid drugs (Figure S10). This specificity eliminates the necessity for employing machine learning techniques to differentiate fentanyl from other opioid drugs.

3. Conclusions

In summary, the distinctive sensing patterns of Au-SWCNT FET devices when exposed to fentanyl and other opioid drugs, including codeine, hydrocodone, and morphine, prompted us to employ a machine learning approach to discriminate fentanyl from other opioids. Utilizing the rich information within the FET transfer characteristics data, we identified 15 features from each sensing dataset for model training, achieving a validation accuracy of 91.2% using LDA. Complementing this, the results of DFT calculations revealed that the sensing capabilities of Au-SWCNT FET sensors toward fentanyl could be attributed to substantially larger interactions and induced electronic changes of this molecule with AuNP-SWCNT relative to the other tested opioid molecules. Additionally, the introduction of specific receptors, *i.e.*, fentanyl antibodies, to the Au-SWCNT FET sensor further expanded the linear range of the FET sensor, and more importantly, enabled intrinsic specificity of the sensor and ultrasensitive detection of fentanyl with a limit of detection as low as 10.8 fg mL^{-1}.

Considering the intricate nature of illicit drug samples in the real world, which may introduce significant interferences to our sensors, identifying and quantifying fentanyl can be particularly challenging. Consequently, we anticipate that a combination of specific and non-specific SWCNT-based FET sensors, coupled with machine learning-supported data analysis, can enhance discrimination across a broader spectrum of drugs at various concentrations. The integration of this sensor array into an automated sensing system holds the potential for high-throughput screening of drug mixtures, offering a highly accurate and efficient approach for analysis of illicit drugs.

4. Experimental Section

Device fabrication. The sensor chips (2.6 mm × 2.6 mm) were fabricated on a Si/SiO_2 wafer, and each contained 8 FET devices. Interdigitated gold electrodes with channel length of 10 μm were patterned on the FET device as source and drain electrodes. Semiconducting single-walled carbon nanotubes (IsoSol-S100, Raymor Industries Inc.) were deposited between the interdigitated electrodes (IDEs) via dielectrophoresis (DEP). The applied bias voltage was 10 V, and the ac frequency was 100 kHz. After a deposition time of 120 s, the sensor chip was annealed at 200 °C for 1 hour before use.

Gold nanoparticles (AuNPs) were decorated on the SWCNTs from a 1 mM $HAuCl_4$ (in 0.1 M HCl) solution via bulk electrolysis. A three-electrode configuration was employed; a 1 M Ag/AgCl electrode was used as the reference electrode, Pt was used as the counter electrode and the IDEs were used as the working electrode. During bulk electrolysis, the voltage was set at –0.2 V and the deposition time was 30 s.

For fentanyl antibody-functionalized Au-SWCNT FET devices, fentanyl antibody solution was prepared at 100 μg mL^{-1} in 1× phosphate buffered saline (PBS) and was added to the surface of sensor chip to allow adsorption of fentanyl antibody on AuNPs. The Au-SWCNT FET devices were incubated with the fentanyl antibody solution for at least 12 hours at 4 °C to ensure maximum immobilization.

Atomic force microscopy (AFM). AFM data was collected using Bruker multimode 8 AFM system with a Veeco Nanoscope IIIa controller in tapping mode. AFM images and height information were obtained in Gwyddion software.

Raman spectroscopy. Raman characterization of the devices was performed using a XplorA Raman-AFM/TERS system. The Raman spectra were recorded using a 638 nm (24mW) excitation laser operating at 10% power.

FET measurements. All FET transfer characteristics were recorded using a Keithley 2602B sourcemeter. The FET measurements were carried out employing a liquid-gated FET configuration, where we collected the source drain current (I_d) under a fixed source drain voltage at 50 mV, while sweeping the gate voltage from +0.6 to −0.6 V versus a 1 M Ag/AgCl reference electrode. The gating media was 0.001× PBS.

All opioid drug solutions, including fentanyl, codeine, hydrocodone, and morphine, were prepared in 1× PBS. The sensing experiment started with the test in the blank solution (PBS), which was used as a baseline for sensor response calculations, and then the opioid drug solutions were tested from the lowest concentration to the highest concentration. For each device, the device was first incubated with 10 μL of each sample for 10 min. After the incubation, unbound analyte was rinsed off with nanopure water, and FET transfer characteristics were collected in the gating media to keep the same ionic strength for all FET measurements.

Fentanyl discrimination with machine learning. Fentanyl, codeine, hydrocodone, and morphine, all prepared at 10 μg mL^{-1}, were used for collecting the sensor responses. The number of devices tested for each drug is 56 for fentanyl, 45 for codeine, 53 for hydrocodone, and 28 for morphine. The FET transfer characteristics of each device before and after the addition of the opioid drug were recorded, and 15 features were extracted from the transfer characteristics curves for model training. The 15 features we identified from the transfer characteristics curves were reported in our previous works.[7c, 7d] A linear discriminant analysis (LDA) model was used for model training, and the classification model accuracy was verified by leave-one-out cross-validation.

Computational Methods. The adsorption properties of fentanyl, codeine, hydrocodone and morphine on Au surface and on hybrid Au-SWCNT system have been determined using dispersion corrected DFT calculations as implemented in the VASP code.[13a, 13b] Calculations were performed using Perdew-Burke-Ernzerhof[19] exchange correlation functional corrected to include long-range dispersion interactions using Grimme-D3[13c] method. Calculations employ the projector augmented wave (PAW) potentials[20] and a plane-wave basis set with a cutoff energy of 400 eV for geometry optimizations which was increased to 500 eV to evaluate the electronic properties. Molecular adsorption on Au(111) surface has been investigated using a 8x3 supercell with its rectangular axes taken along crystallographic directions $[1,0,\bar{1}]$ and $[\bar{1},2,\bar{1}]$. This slab model contains four Au layers with the bottom two layers frozen at the bulk optimized dimensions while the top two layers were fully relaxed. A vacuum layer of 27.8 Å was considered in these calculations to decouple the lateral interactions among successive cells in a direction perpendicular to the surface. For Au adatom mediated adsorption studies the corresponding slab model contained an additional Au adatom on Au(111) surface. Given the relative large size of the supercell used structural optimizations were performed using a 1x1x1 Monkhorst-Pack[21] grid to sample the Brillouin zone. For the hybrid AuNP-SWCNT system, the corresponding slab model consists of a Au80 nanoparticle adsorbed on a (14,0) SWCNT with six repeated units taken along the Oy axis of the supercell. This SWCNT contains a C-C defect which was functionalized with a mixture of COOH, O and H species. For structural optimizations of this hybrid AuNP/SWCNT system a single G point was used while a finer 1x7x1 Monkhorst-Pack grid was considered for evaluation of the electronic properties. The adsorption energies were determined based on the expression $E_{ads}=E_{molec}+E_{slab}-E_{(molec+slab)}$ where E_{molec} is the energy of the isolated adsorbate molecule in gas phase, E_{slab} is the total energy of the slab and $E_{(molec+slab)}$ is the total energy of adsorbate-slab system.

In this sign convention a positive adsorption energy corresponds to a stable configuration. Finally, the amount of charge transferred among different subsystems of the fentanyl-AuNP-SWCNT hybrid system was obtained based on the Bader charges[22] evaluated using Henkelman *et al.*[23] algorithm.

Statistical Analysis. The FET sensor responses were calculated using the equation $R = \Delta I/I_0$ at $V_g = -0.3$ V, where I_0 is the I_d at −0.3 V in the blank sample (baseline), and ΔI is the difference in I_d between the sample and the blank. The calibration curve was constructed by plotting the averaged relative conductance of all devices against the concentration of the analyte on a logarithmic scale. The error bars reported in the calibration curve represented the standard error of the relative responses of all FET devices tested. The number of devices (*n*) was indicated in Figures 2 and 4 in the main text.

To determine the linear range of the sensor, the calibration curve was fitted using a logistic model and the linear region of the fitted curve was identified as the linear range. Calibration sensitivity was defined as the slope of the linear region in the calibration curve.

To determine the dissociation constant (K_d) for the adsorption of fentanyl on AuNPs, $\frac{[\text{Fentanyl}]}{|\text{Rel.response}|}$ was plotted as a function of [Fentanyl], where [Fentanyl] is the concentration of fentanyl in fg mL^{-1} and $|\text{Rel. response}|$ is the absolute relative response at −0.3 V. A linear relationship was obtained, indicative of Langmuir isotherm adsorption. K_d was then calculated using the equation $\frac{[\text{Fentanyl}]}{|\text{Rel. response}|} = \frac{1}{|\text{Rel. response}|_{\text{max}}}[\text{Fentanyl}] + \frac{K_d}{|\text{Rel. response}|_{\text{max}}}$. On the other hand, the dissociation constant (K_d) for fentanyl-fentanyl antibody binding was extracted from the calibration curve as the analyte concentration at half-maximum sensor response.[17, 24]

The limit of detection was calculated according to the International Union of Pure and Applied Chemistry (IUPAC) definition.[25] Firstly, we determined the smallest sensor response that can be detected with reasonable certainty, x_L, by using the equation $x_L = \bar{x}_B + ks_B$. Here, $\bar{x}_B$ is the mean of the blank measures, s_B is the standard deviation of the blank measures, and k is 3 for a confidence of 99.6%. From the calibration curve shown in Figure 4b, we found $\bar{x}_B = 0.02607$, $s_B = 0.00784$, and $x_L = 0.00496$. Then, the concentration of fentanyl corresponding to this x_L (LOD) was interpolated from the fitted calibration curve.

References

[1] Y. Han, W. Yan, Y. Zheng, M. Z. Khan, K. Yuan, L. Lu, *Transl. Psychiatry* **2019**, *9*, 282.

[2] a) P. Armenian, K. T. Vo, J. Barr-Walker, K. L. Lynch, *Neuropharmacology* **2018**, *134*, 121–132; b) K. B. Palmquist, M. T. Truver, E. N. Shoff, A. J. Krotulski, M. J. Swortwood, *J. Forensic Sci.* **2023**, *68*, 1643–1661.

[3] a) R. A. Crocombe, G. Giuntini, D. W. Schiering, L. T. M. Profeta, M. D. Hargreaves, P. E. Leary, C. D. Brown, J. W. Chmura, *J. Forensic Sci.* **2023**, *68*, 1570–1600; b) A. Weber, B. Hoplight, R. Ogilvie, C. Muro, S. R. Khandasammy, L. Perez-Almodovar, S. Sears, I. K. Lednev, *Anal. Chem.* **2023**, *95*, 167–205.

[4] a) A. N. Masterson, S. Hati, G. Ren, T. Liyanage, N. E. Manicke, J. V. Goodpaster, R. Sardar, *Anal. Chem.* **2021**, *93*, 2578–2588; b) H. Wang, Z. Xue, Y. Wu, J. Gilmore, L. Wang, L. Fabris, *Anal. Chem.* **2021**, *93*, 9373–9382; c) N. G. Wilson, J. Raveendran, A. Docoslis, *Sens. Actuators B Chem.* **2021**, *330*; d) L. Wang, M. O. Vendrell-Dones, C. Deriu, S. Dogruer, B. H. P. de, B. McCord, *Appl. Spectrosc.* **2021**, *75*, 1225–1236; e) M. M. Kimani,

A. Lanzarotta, J. S. Batson, *J. Forensic Sci.* **2021**, *66*, 491–504; f) M. Zhang, J. Pan, X. Xu, G. Fu, L. Zhang, P. Sun, X. Yan, F. Liu, C. Wang, X. Liu, G. Lu, *Anal. Chem.* **2022**, *94*, 4850–4858; g) X. Su, X. Liu, Y. Xie, M. Chen, H. Zhong, M. Li, *Anal. Chem.* **2023**, *95*, 3821–3829; h) X. Li, L. Sun, B. Xu, L. Dai, Y. Xiao, Y. Ding, Q. Liu, M. Meng, R. Xi, L. Guo, Y. Yin, *Sens. Actuators B Chem.* **2023**, *385*.

[5] a) M. W. Glasscott, K. J. Vannoy, P. U. A. Iresh Fernando, G. K. Kosgei, L. C. Moores, J. E. Dick, *TrAc - Trends Anal. Chem.* **2020**, *132*, 116037; b) Z. Dai, *Sensors (Basel)* **2023**, *23*, 3140.

[6] G. O. Silva, Z. P. Michael, L. Bian, G. V. Shurin, M. Mulato, M. R. Shurin, A. Star, *ACS Sens.* **2017**, *2*, 1128–1132.

[7] a) L. Bian, D. C. Sorescu, L. Chen, D. L. White, S. C. Burkert, Y. Khalifa, Z. Zhang, E. Sejdic, A. Star, *ACS Appl. Mater. Interfaces* **2019**, *11*, 1219–1227; b) L. Bian, Z. Wang, D. L. White, A. Star, *Biosens. Bioelectron.* **2021**, *180*, 113085; c) Z. Liu, G. V. Shurin, L. Bian, D. L. White, M. R. Shurin, A. Star, *Anal. Chem.* **2022**, *94*, 3565–3573; d) Z. Liu, L. Bian, C. J. Yeoman, G. D. Clifton, J. E. Ellington, R. D. Ellington-Lawrence, J. C. Borgogna, A. Star, *Anal. Chem.* **2022**, *94*, 3849–3857.

[8] a) Z. P. Michael, W. Shao, D. C. Sorescu, R. W. Euler, S. C. Burkert, A. Star, *J. Phys. Chem. C* **2017**, *121*, 20813–20820; b) S. Mubeen, T. Zhang, N. Chartuprayoon, Y. Rheem, A. Mulchandani, N. V. Myung, M. A. Deshusses, *Anal. Chem.* **2010**, *82*, 250–257.

[9] Z. Ding, C. Wang, X. Song, N. Li, X. Zheng, C. Wang, M. Su, H. Liu, *ACS Appl. Mater. Interfaces* **2023**, *15*, 12570–12579.

[10] X. Liang, N. Li, R. Zhang, P. Yin, C. Zhang, N. Yang, K. Liang, B. Kong, *NPG Asia Mater.* **2021**, *13*, 8.

[11] Y. Chen, H. Vedala, G. P. Kotchey, A. Audfray, S. Cecioni, A. Imberty, S. Vidal, A. Star, *ACS Nano* **2012**, *6*, 760–770.

[12] a) I. Heller, A. M. Janssens, J. Mannik, E. D. Minot, S. G. Lemay, C. Dekker, *Nano Lett.* **2008**, *8*, 591–595; b) R. J. Chen, H. C. Choi, S. Bangsaruntip, E. Yenilmez, X. Tang, Q. Wang, Y.-L. Chang, H. Dai, *J. Am. Chem. Soc.* **2004**, *126*, 1563–1568.

[13] a) G. Kresse, J. Furthmüller, *Comput. Mater. Sci.* **1996**, *6*, 15-50; b) G. Kresse, J. Furthmüller, *Phys. Rev. B* **1996**, *54*, 11169-11186; c) S. Grimme, J. Antony, S. Ehrlich, H. Krieg, *J. Chem. Phys.* **2010**, *132*, 154104-154119.

[14] B. Ban, R. C. Barrientos, T. Oertel, E. Komla, C. Whalen, M. Sopko, Y. You, P. Banerjee, A. Sulima, A. E. Jacobson, K. C. Rice, G. R. Matyas, V. Yusibov, *MAbs* **2021**, *13*, 1991552.

[15] Y. Zhang, O. Pluchery, L. Caillard, A. F. Lamic-Humblot, S. Casale, Y. J. Chabal, M. Salmeron, *Nano Lett.* **2015**, *15*, 51–55.

[16] S. N. Kim, J. F. Rusling, F. Papadimitrakopoulos, *Adv. Mater.* **2007**, *19*, 3214–3228.

[17] W. Shao, Z. Zeng, A. Star, *ACS Appl. Mater. Interfaces* **2023**, *15*, 37784–37793.

[18] a) L. C. Smith, P. T. Bremer, C. S. Hwang, B. Zhou, B. Ellis, M. S. Hixon, K. D. Janda, *J. Am. Chem. Soc.* **2019**, *141*, 10489–10503; b) D. Hicks, C. Baehr, P. Silva-Ortiz, A. Khaimraj, D. Luengas, F. A. Hamid, M. Pravetoni, *Hum. Vaccin. Immunother.* **2022**, *18*, e2122507; c) J. V. Rodarte, C. Baehr, D. Hicks, T. L. Liban, C. Weidle, P. B. Rupert, R. Jahan, A. Wall, A. T. McGuire, R. K. Strong, S. Runyon, M. Pravetoni, M. Pancera,

Structure **2023**, *31*, 20–32; d) P. T. Bremer, E. L. Burke, A. C. Barrett, R. I. Desai, *Nat. Commun.* **2023**, *14*, 7700.

[19] J. P. Perdew, K. Burke, M. Ernzerhof, *Phys. Rev. Lett.* **1996**, *77*, 3865-3868.

[20] P. E. Blöchl, *Phys. Rev. B* **1994**, *50*, 17953-17979.

[21] H. J. Monkhorst, J. D. Pack, *Phys. Rev. B* **1976**, *13*, 5188-5192.

[22] R. F. W. Bader, *Atoms in Molecules A Quantum Theory*, Oxford University Press, New York, USA, **1994**.

[23] E. Sanville, S. D. Kenny, R. Smith, G. Henkelman, *J. Comput. Chem.* **2007**, *28*, 899-908.

[24] a) J. A. Eble, *J. Vis. Exp.* **2018**, e57334; b) J. Paakkonen, J. Janis, J. Rouvinen, *ACS Omega* **2022**, *7*, 10789−10795; c) W. Shao, G. V. Shurin, X. He, Z. Zeng, M. R. Shurin, A. Star, *ACS Appl. Mater. Interfaces* **2022**, *14*, 1684–1691.

[25] in *IUPAC Compendium of Chemical Terminology*, 3 ed., International Union of Pure and Applied Chemistry (IUPAC), **2019**.